SPATIAL RAINBOWS AND CATASTROPHES IN TRANSMISSION OF PROTONS THROUGH THE ELECTROSTATIC OCTOPOLE LENS

by

Igor N. TELEČKI*, Sanja M. GRUJOVIĆ ZDOLŠEK, and Srdjan M. PETROVIĆ

Laboratory of Physics, Vin~a Institute of Nuclear Sciences, University of Belgrade, Belgrade, Serbia

Scientific paper
http://doi.org/10.2298/NTRP180910008T

This paper considers the transmission of the initial parallel proton beam with kinetic energy of 10 keV through the electrostatic octopole lens. The spatial rainbows and corresponding proton distributions are calculated by using the infinite length approximation potential. Positive potentials of the lens electrodes are set to be 0.35 kV and 9 kV. It has been shown that by application of catastrophe theory, the generating function for mapping proton positions between entrance and exit transverse plains can be determined, giving accurate rainbow patterns for biasing potentials of 0.35 kV.

Key words: octopole, beam optics, catastrophe theory, rainbow line, aberration

INTRODUCTION

A perfect 2-D octopole electric field may be generated by an electrode structure consisting of eight infinitely long parallel rods of the hyperbolic cross-section, with rod centers equally spaced around a circle. The electrodes are set to be on alternating electrostatic potentials V_0 [1-3]. Octopole effect on charged beam particles primarily introduces a third-order path deviation resulting in a fourfold third-order deformation of a rotationally symmetric beam [4]. This deviation, according to aberration classification nomenclature, corresponds to four-fold astigmatism. The secondary path deviations are of the fifth- order. Octopoles are used in reduction of third-order spherical aberrations, mainly in electron microscopy. Combined positive spherical aberrations of quadrupoles and four-fold astigmatism of octopoles, forming a negative spherical aberration, can be used for correction of a positive spherical aberration of the objective lens in electron microscopy [5-7].

In the previous study [8] we have shown that spatial rainbow lines, determined numerically by calculation of proton trajectories propagating through and after the hexapole lens, can be successfully used for fitting corresponding generating function for this lens. Since the generating function is related to geometric aberrations, it also determines optical properties of the observed hexapole lens.

In this work, we performed a similar study for an octopole electrostatic lens, which is very often used as a complementary lens with the hexapole one. The transmission of a parallel 10 kV proton beam through the lens and the corresponding rainbow lines were considered. Two values of the biasing potential of the lens electrodes were chosen: $V_0 = 0.35$ and 9 kV. Applying the same technique as described in [8], a generating function that characterizes the mapping process, for $V_0 = 0.35$ kV, was fitted. In addition to this, expression for the beam transmission coefficient k_t as a function of the potential V_0 was derived.

THEORY

For an infinitely extended octopole lens, as shown in fig. 1, the electrostatic potential in vacuum for hyperbolic-shape electrodes, can be written as [1, 2]

$$\varphi(x, y) \quad \frac{V_0}{r_0^4}(x^4 \quad 6x^2 y^2 \quad y^4) \tag{1}$$

where V_0 denotes the applied positive electrode potential and r_0 the radius of a circle inscribed within eight electrodes. It is readily verified that this function satisfies Laplace's equation $\varphi(x, y) = 0$. From the symmetric and anti-symmetric properties of the potential, the following relations hold: $\varphi\ -x, y \quad \varphi(x, y)$ or $\varphi(x, -y \quad \varphi(x, y)$ and (under 45° rotation around the lens axis) $\varphi((x \quad y)/\sqrt{2}, (x \quad y)/\sqrt{2}) \quad \varphi(x, y)$. Moreover, provided that the radius d of each rod is related to the radius r_0 of the inscribed circle (see fig. 1) according to

$$r_0 \quad \frac{N}{2} \quad 1 \quad d \tag{2}$$

* Corresponding author; e-mail: tigor@vin.bg.ac.rs

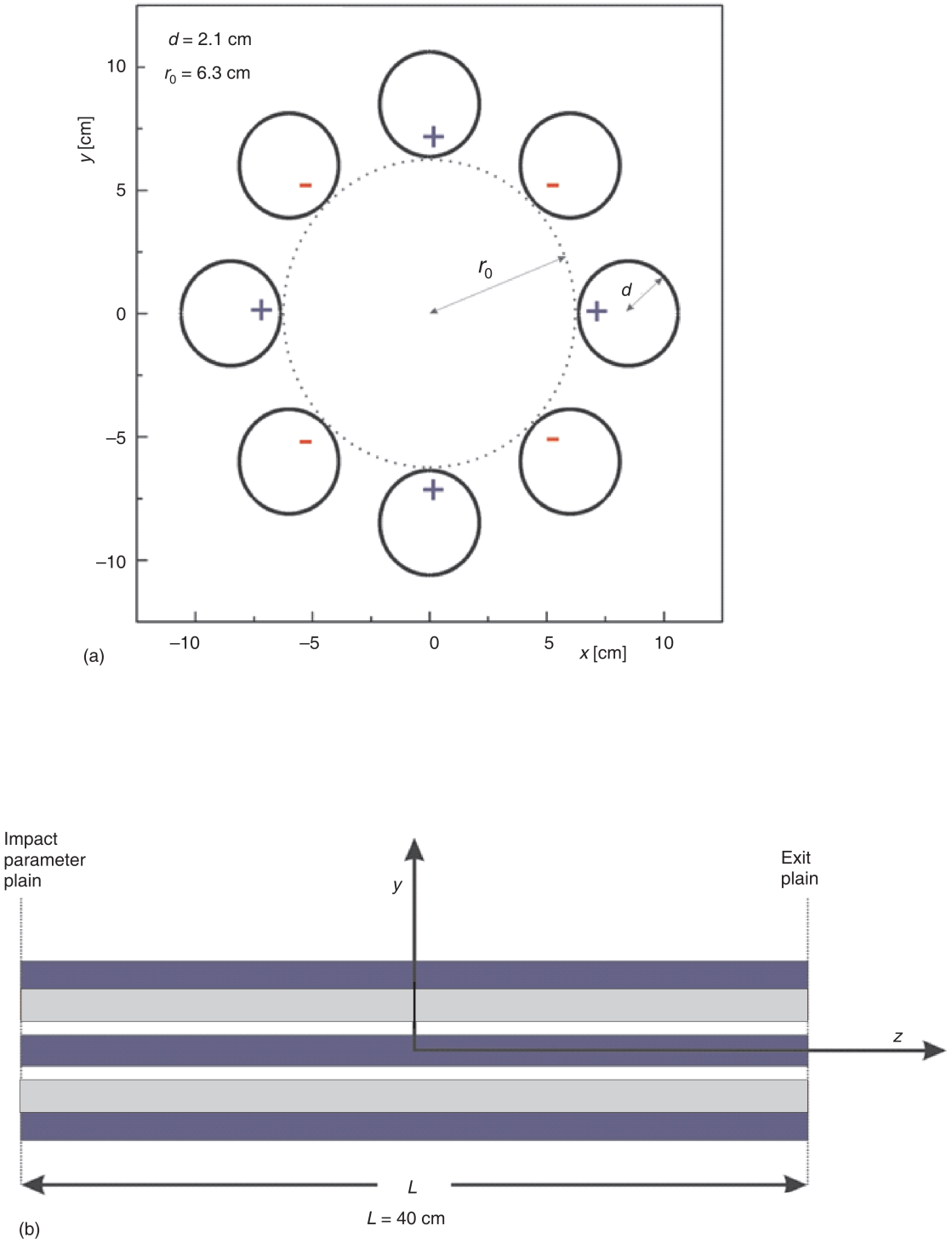

Figure 1. (a) The medium transverse position plain of the octopole lens, (b) longitudinal cross-section of the lens: the blue and red colors (dark and gray) of electrodes correspond to the positive and negative applied potential

where $N > 4$ is the number of poles of a multipole, then the potential generated by rods of the hyperbolic cross-section is very well approximated by rods of the circular cross-section [2]. For an octopole ($N = 8$ in eq. (2)), we should therefore choose $r_0 = 3d$. The corresponding electric field components are

$$E_x(x, y) \quad \frac{4V_0}{r_0^4}(x^3 \quad 3xy^2) \tag{3a}$$

$$E_y(x, y) \quad \frac{4V_0}{r_0^4}(y^3 \quad 3yx^2) \tag{3b}$$

The motion of a proton in the presence of this electric field is fully described by

$$\frac{d^2 r}{dz^2} \quad \frac{q_p}{v_z m_p}\boldsymbol{E}(r) \quad \frac{4V_0}{r_0^4}\frac{q_p}{v_z m_p} \begin{matrix} (x^3 & 3xy^2)e_x \\ (y^3 & 3yx^2)e_y \\ & 0\,e_z \end{matrix} \tag{4}$$

where m_p, q_p, and v_z are the mass, charge, and longitudinal velocity of the proton, respectively, and **r** is the transverse proton position. The variables in eq. (4) cannot be separated *i. e*., it cannot be solved analytically. Therefore the proton trajectories were calculated by using the fourth-order Runge-Kutta [9] numerical integration of eq. (4).

Let us now consider the mapping of two neighboring trajectories in the same transverse plain at the longitudinal position z

$$\begin{matrix} x_0 \\ y_0 \end{matrix} \mapsto \begin{matrix} x(x_0, y_0, z) \\ y(x_0, y_0, z) \end{matrix} \text{ and}$$

$$\begin{matrix} x_0 & \mathrm{d}x_0 \\ y_0 & \mathrm{d}y_0 \end{matrix} \mapsto \begin{matrix} x(x_0 & dx_0, y_0 & \mathrm{d}y_0, z) \\ x(x_0 & dx_0, y_0 & \mathrm{d}y_0, z) \end{matrix} \quad (5)$$

where the starting positions (x_0, y_0), and $(x_0 + ,\mathrm{d}x_0 y_0 + + \mathrm{d}y_0)$ are in the impact parameter (IP) plain, while $(x(x_0, y_0, z), y(x_0, y_0, z))$ and $(x(x_0 + \mathrm{d}x_0, y_0 + \mathrm{d}y_0, z), y(x_0 + + \mathrm{d}x_0, y_0 + \mathrm{d}y_0, z))$ are the proton spatial components after its motion through the lens and/or after it, at the transversal position (TP) plain. In fig. 1(b) the IP plain it is set to be at the entrance of the octopole lens, while the TP plain coincides with the exit plain of the lens. It should be noted that it has no fixed position along the axis of the lens. The mapping process between the IP plain and the TP plain, given by eq. (5) is defined by the Jacobian of the transverse components of the proton position vector, which reads

$$J_\rho(x_0, y_0, z) \quad \partial_{x_0} x \partial_{y_0} y \quad \partial_{x_0} x \partial_{y_0} y \quad (6)$$

The Jacobian can be considered as a transfer function defining the mapping of a small area $\mathrm{d}x_0\,\mathrm{d}y_0$ in the IP plain into a correspondingly small area $\mathrm{d}x\mathrm{d}y$ of the TP plain. *i. e*. $\mathrm{d}x\mathrm{d}y = J_\rho(z)\mathrm{d}x_0\,\mathrm{d}y_0$. Therefore, reciprocal of Jacobian determinant is proportional to intensity of proton beam at the position of TP plain.

The condition $J_\rho = 0$ should give the shape of the rainbow line (RL) in the IP plain along which this mapping is singular. In general, the mapping defined by eq. (5) is not an injective (one-to-one correspondence) function *i. e*. two or more neighboring rays could intersect each other at the TP plain, which often leads to so-called catastrophic phenomena. In the context of ion beam optics, the term catastrophic symbolizes the singularity of protons intensity along RL, which represents the border between the so-called bright and dark sides of the rainbow [8, 10-13].

RESULTS AND DISCUSSION

In our calculations the radii of each six electrodes are set up to be $d = 2.1$ cm. Due to the restrictions imposed by eq. (2), the radius of the circle inscribed within the electrodes is equal to $r_0 = 3d = 6.3$ cm. The polarity

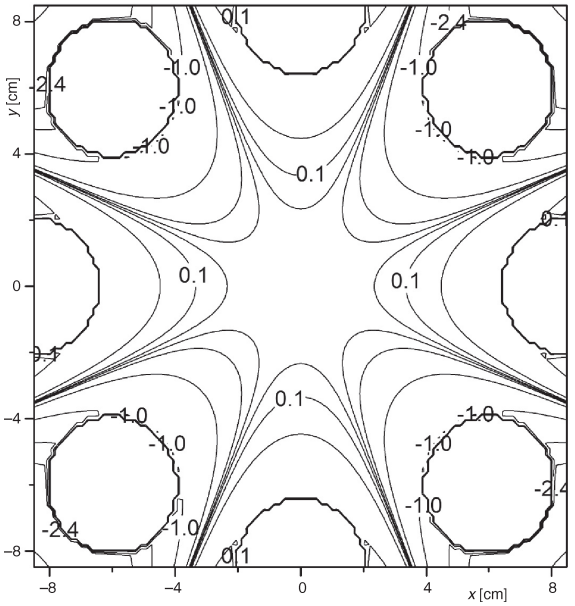

Figure 2. Electrostatic potential distribution over the chosen octopole geometry, for electrode biasing voltage of $V_0 = 1$V

of the electrodes is shown in fig. 1(a). The length of the electrodes is $L = 40$ cm. The origin of the used coordinate system is taken to be in the middle of the octopole lens, and the z axis coincides with the lens axis (see fig. 1(b)). The positions of the entrance and exit transversal plains shown in fig. 1(b) correspond to the longitudinal co-ordinate $z = –20$ cm and $z = 20$ cm, respectively. The proton energy is taken to be $E = 10$ keV whereas the initial number of protons taken into the simulation is 600 000. The initial proton beam is parallel to the lens axis, homogenously distributed within the diameter of a circle equal to 4 cm, laying onto the IP plain. A circular aperture, 6 cm in diameter, is set up at exit plain. The horizontal and vertical coordinates, x and y, respectively, are chosen so that the proton beam is directed towards the direction of the z axis, which coincides with the lens axis.

The distribution of the electrostatic potential over an arbitrary TP, far enough from the lens edges, for biasing potential of $V_0 =$ 1 V is presented in fig. 2. Each of the eight pole pieces has the same shape and so the structure is unchanged under a 45° rotation. The inner equipotential lines, which are close to the electrodes, have almost a circular shape, becoming more and more hyperbolic with greater distance from the electrodes. Since electrode structure of a real lens is not infinitely long, the electrostatic field/potential distribution depends not solely on the transverse (x and y), but also on longitudinal (z) co-ordinate. This fact is particularly pronounced at the extremities of the electrode structure (entrance and exit transverse plain) where the well-known effect of the fringe field appears. However, the infinite length potential approximation, given by eq. (1), is acceptable for the real lens if the length L is much longer than its diameter r_0. In

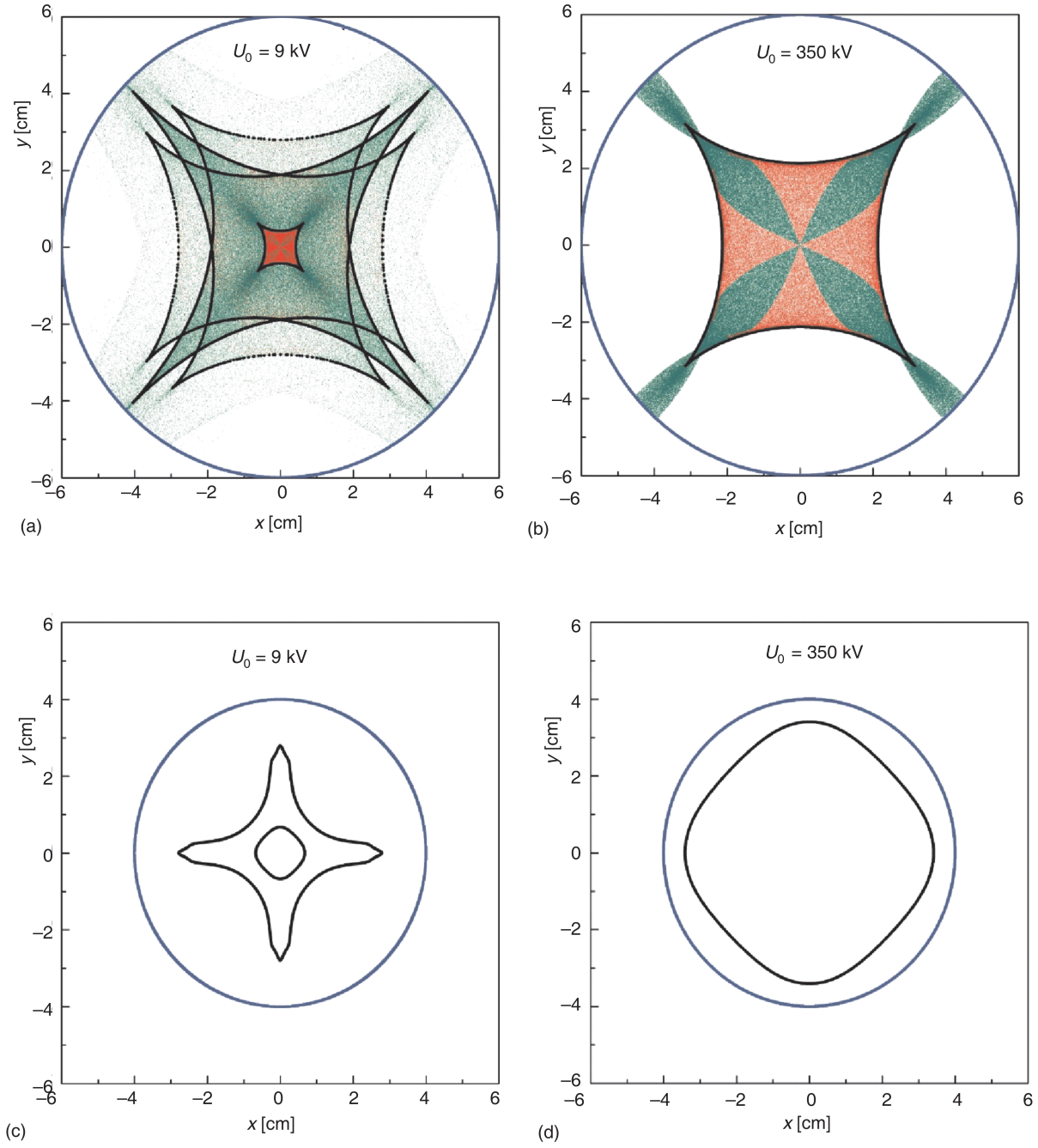

Figure 3. Rainbow lines in the impact parameter plain for (a) V_0 = 9 kV , (c) V_0 = 0.35 kV, and corresponding mapped images in the exit transverse plain, together with spatial distribution of transmitted protons for (b) V_0 = 9 kV and (d) V_0 = 0.35 kV. The red and green (dark and gray) points designate the focused and defocused protons, respectively. The blue (grey) circle represents the exit lens aperture

our case L is more than six times longer than r_0, which justifies our use of this approximation.

The biasing voltage on the electrodes at which RL form closed lines in both IP and TP plains, is called characteristic voltage. Figure 3 presents two such cases, for two characteristic voltages of 0.35 kV and 9 kV. In case of lower potential, the corresponding RL in TP and IP plains are shown in fig. 3(c) and 3(d), respectively. The blue circular lines represent the entrance/exit lens aperture (alternative, the gray designation color is used in the printed version). It should be emphasized that RL in the IP plain is not an observable phenomenon. It only determines the initial protons positions that are mapped into the corresponding RL in the defined TP plain, the latter being observable experimentally. In this case the virtual rainbow line in the IP plain (the black round line) is being mapped into the black cusp square in the TP plain.

The red and green color points (alternative dark and gray designation colors are used in the printed version of the journal) designate the focused and defocused transmitted protons, respectively. The protons are focusing if during their movement they are approaching the axis of the lens. Otherwise they are

defocusing [8, 10-13]. If during the propagation a proton hits some of the electrodes or apertures, it is considered lost for further transmission. The initial circular beam at the IP plain is deformed by a square cusp at the exit of the lens, so that the proton yield changes rapidly across the RL. The common term of the dark and bright side of the rainbow, here actually corresponds to areas of low proton yield that are outside, and the high proton yield that are inside the RL. Having this in mind, one can conclude that the rainbow lines play the role of skeletons or structure of the beam shape. This is an obvious manifestation of the catastrophic character of the proton beam dynamics in the lens [8, 10-13]. While the focused protons are confined within RL, the defocused ones migrate from the bright side of the rainbow to its dark side, mainly through the cusps of the RL.

For the characteristic potential of $V_0 = 9$ kV, the process of mapping is more complex. In addition to the square cusp shape, a secondary complex 12 cusped RL in the TP plain appears, as shown in fig. 3 (a). These two RL are images of the corresponding lines in the IP plain depicted in fig. 3(b): the inner circular-like line is mapped into the square cusped RL, while the mapping of the outer cross-like line gives the secondary complex 12 cusped RL. In this case the RL in the TP plain also present skeletons of the transmitted ion beam distribution. One can conclude, as being evident from fig. 3(a), that both RL serve as a confinement borders for the proton beam. Judging by the density of the proton distribution, the confining ability of the inner (or primary) RL is much stronger in comparison to the outer (or secondary) one. In addition to this, the inner RL confines mostly the focused protons, while the outer RL defines the part of the beam consisting mostly of defocused protons.

The particle beams with an underlying RL (instead of RL, most often in literature the term caustic is used) structure are stable under perturbation, if the RL belongs to the catastrophe-theory classification (fold, cusp, swallowtail, hyperbolic and elliptic umbilic, *etc*.) [14]. Each RL singularity, and its corresponding catastrophe, is described by a canonical form generated from an elementary polynomial [15].

Generating function of an octopole is

$$F(x_0 y_0; x, y, z) \quad \frac{1}{2}(x_0^2 \quad y_0^2) \quad (x_0 x \quad y_0 x) \quad \frac{1}{4} a(z)(x_0^4 \quad 6x_0^2 y_0^2 \quad y_0^4) \quad \frac{1}{6} b(z)(x_0^6 \quad 3x_0^4 y_0^2 \quad 3x_0^2 y_0^4 \quad y_0^6) \tag{7}$$

The first and second term correspond to the particle co-ordinates without path deviation, *i. e*., movement in field-free space [16], the third and fourth terms correspond to fourfold umbilic and rotational cusp catastrophes [4, 15-17]. It should be noted that the third term of the generating function is related to the astigmatism of the third-order whereas the fourth term is related to the spherical aberration of the fifth-order [18]. The last two terms introduce a third- and fifth-order path deviation on charged particle trajectories.

The generating function defines the following polynomial nonlinear mapping, $x_0 y_0 \quad x, y$, via the relations

$$\partial_{x_0} F(x_0, y_0; x, y, z) \quad 0 \quad x \quad x_0 \quad a(z)(x_0^3 \quad 3x_0 y_0^2) \quad b(z)(x_0^5 \quad 2x_0^3 y_0^2 \quad x_0 y_0^4) \tag{8}$$

$$\partial_{y_0} F(x_0, y_0; x, y, z) \quad 0 \quad y \quad y_0 \quad a(z)(y_0^3 \quad 3y_0 x_0^2) \quad b(z)(y_0^5 \quad 2y_0^3 x_0^2 \quad y_0 x_0^4) \tag{9}$$

According to catastrophe theory, the conditions (7) and (8) define the equilibrium set of the family of functions, F [18]. It can be shown that the Jacobian of the 2-D mapping defined as $J_\rho^m(x_0, y_0; x, y, z) = \partial_{x_0}^2 F \, \partial_{y_0}^2 F \quad (\partial_{x_0} \partial_{y_0} F)^2$ is given by

$$J_\rho^m(x_0, y_0; x, y, z) \quad 1 \quad (9a^2(z) \quad 6b(z))x_0^4 \quad (9a^2(z) \quad 6b(z))y_0^4 \quad (18a^2(z) \quad 12b(z)x_0^2 y_0^2 \quad 12a(z)b(z)x_0^6 \quad 12a(z)b(z)y_0^6 \quad 60a(z)b(z)x_0^4 y_0^2 \quad 60a(z)b(z)x_0^2 y_0^4 \quad 5b^2(z)x_0^8 \quad 5b^2(z)y_0^8 \quad 30b^2(z)x_0^4 y_0^4 \quad 20b^2(z)x_0^2 y_0^6 \quad 20b^2(z)x_0^6 y_0^2 \tag{10}$$

which represents, on the other hand, the Hessian of the generating function, H (F) [17]. According to catastrophe theory, equation, H (F) = 0, which is equivalent to the condition defining the spatial rainbow lines in the IP plain, corresponds to the catastrophic set of the family of functions F. The bifurcation set of the family F is defined as the mapping of the catastrophic set via the eqs. (8) and (9) [17], and, therefore, corresponds to the rainbow lines in the TP plain. Thus, we have shown a direct connection between the rainbow lines in the IP and TP plains and the catastrophic and bifurcation sets of the generating function (7), respectively.

As mentioned earlier, the equation $J_\rho = 0$ defines the rainbow lines. Depending on the way of determining the Jacobian of the mapping, in this study we consider two cases. The first one is when the mapping is determined by the numerically calculated electrostatic potential of the octopole lens. The solving of the mapping equation is done by numerical methods *i. e*. by numerical integration of the proton's equations of motion. The resulting RL in this case are called numerical RL. In the second case, we use the analytical potential given by eq. (1), and consequently, the mapping equation $J_\rho^m \quad 0$ is the polynomial given in on the right-hand side of equation (10). The RL obtained in this way are called model RL. Since the numerical solution of this problem is complicated and time con-

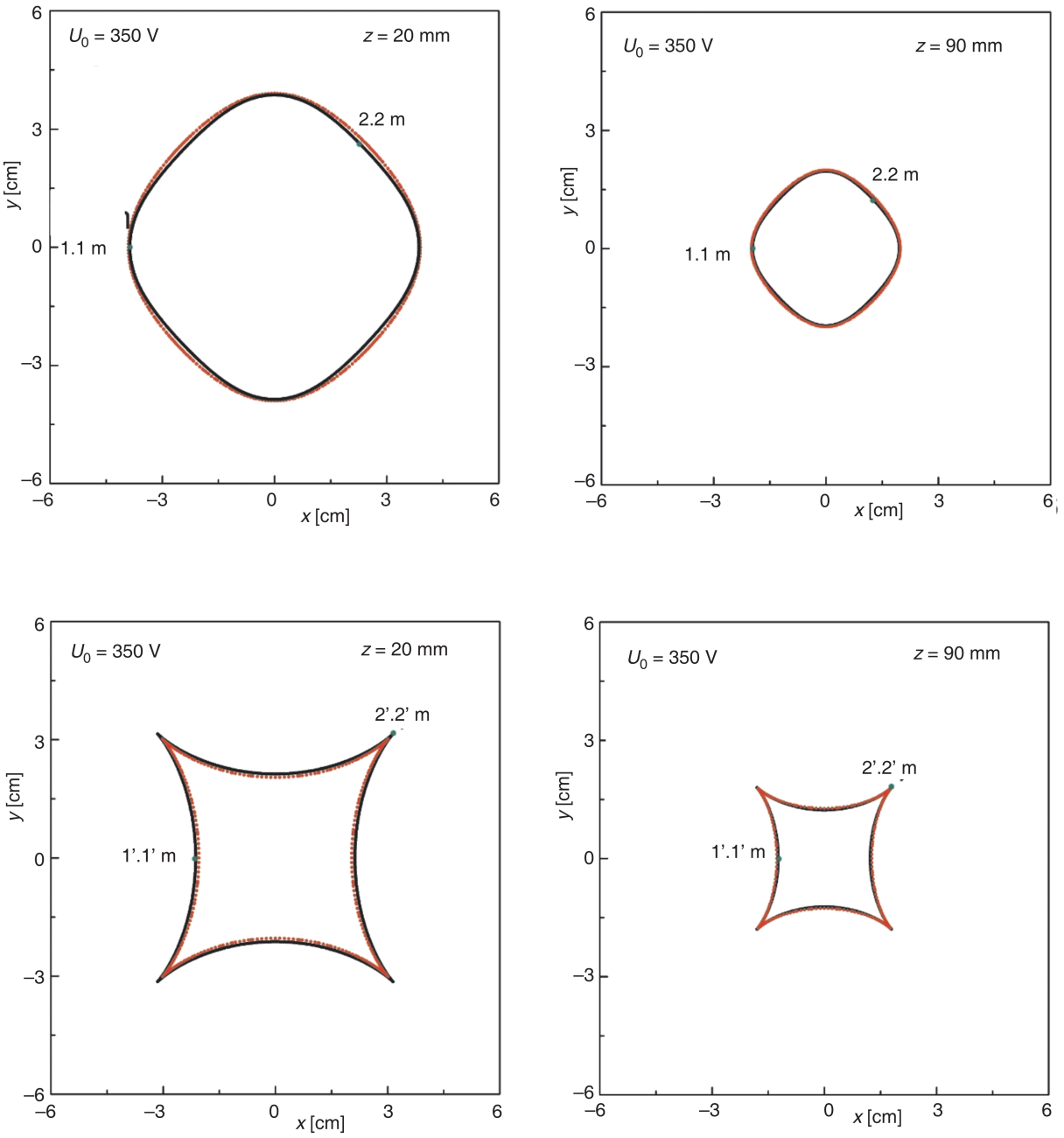

Figure 4. The analytical (black color) and numerical (red/gray) color rainbow lines in IP plain shown in (a) and (c), and the corresponding rainbow lines in the exit plain, for $z = 20$ cm (b), and in drift space for $z = 90$ cm (d). The electrode biasing potential is $V_0 = 0.35$ kV

suming, it will be shown that the model RL are a good approximation of the numerical ones.

The unknown parameters a (z) and b (z) appearing in eqs. (7)-(10), are determined in the fitting procedure, at points laying on the z axis of the lens. This approach provides the best match between the corresponding numerical and model rainbow lines, in both IP and TP plains [8]. Figure 4 shows the numerically calculated RL (red line) and the corresponding best fitting model RL (black line), both in the IP and TP plains, respectively, for biasing the potential of V_0 = 0.35 kV. Two cases, for z equal to 20 cm and 90 cm are shown. In the first case, the TP plain is within the lens, while in the second one, it is in the drift space, 50 cm behind the exit edge of the lens. The fitting procedure for determining a (z) and b (z) is achieved by minimizing the sum of squared distances between the corresponding points $1(x_{01}, y_{01})$ and $1_m(x_{01m}, y_{01m})$, $2(x_{02}, y_{02})$ and $2_m(x_{02m}, y_{02m})$ in the IP plain, and $1'(x_1, y_1)$ and $1'_m(x_{1m}, y_{1m})$, and, $2'(x_2, y_2)$ and $2'_m(x_{2m}, y_{2m})$, and the TP plain, that are presented in fig. 4. The mentioned fitting criterion is given by

$$\min \sum_{i=1}^{2} (x_{0i} - x_{0im})^2 + (y_{0i} - y_{0im})^2 + (x_i - x_{im})^2 + (y_i - y_{im})^2 \qquad (11)$$

where, the additional index *m* denotes the points on the model RL to distinguish them from numerically calculated RL points. The intersection points for both RL with the *x* axis we denote with 1, while 2 denotes the points on top of the cusp. The chosen points give excellent matches. For example, the minimal squares of deviations obtained for $z = 20$ cm and $z = 90$ cm (cases shown in in fig. (4) give the averaged difference between RL in both plains of 1 % and 10^{-1}%, respectively. The same procedure is applied for the values of variable $z = 50, 60, 70, 80, 90, 100, 120, 140, 160, 180,$ and 200 cm *i. e.*, within the drift space behind the lens. The corresponding obtained values of parameters *a* and *b* are presented in figs. 5(a) and 5(b), respectively. The analysis shows that dependences of parameters *a* and *b* on variable *z* can be excellently fitted with the following analytical functions, $a(z) = a_1 - a_2 \exp(-z/a_z)$ and $b(z) = b_1 - b_2 \exp(-z/b_z)$, respectively. Calculated parameters of the fitting functions are: $a_1 = 0.26$ cm^{-1}, $a_2 = 0.54$ cm^{-1}, and $a_z = 29.10$ cm, and $b_1 = 0.09$ cm^{-2}, $b_2 = 0.25$ cm^{-2}, and $b_z = 37.18$ cm.

Figure 6 gives the transmission coefficient of the lens, k_t, as a function of the biasing potential V_0, varying between 0.35 and 9 kV *i. e.* between the characteristic potentials at which the first and the second RL are represent by closed lines. This parameter of the lens is defined as the ratio of the number of transmitted protons in the exit plain of the lens and the initial number of protons in the IP plain. One should note that k_t decreases with the increase of the potential on electrodes. For $V_0 = 0.35$ kV the value of k_t is 0.75 and for $V_0 = 9$ kV k_t it falls to 0.17 *i. e.* it is 4.5 times lower. Analysis shows that dependency of k_t on V_0 can be fitted by an exponential function $k_t(V_0) = k_1 + k_2 \exp(-V_0/k_{V_0})$, where the values of the fitting parameters are $k_1 = 0.18$, $k_2 = 0.65$, and $k_{V_0} = 2$ kV.

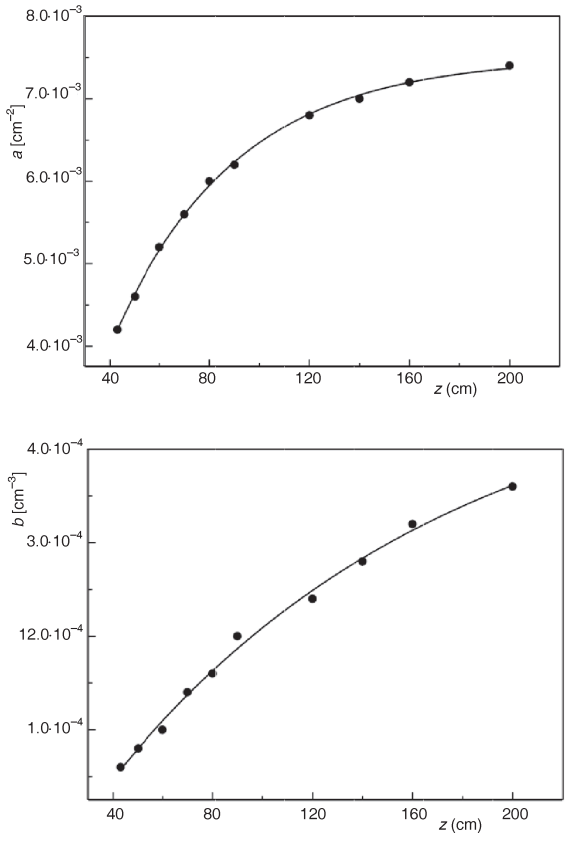

Figure 5. Dependencies of the fitting parameters (a) *a*, and (b) *b*, on variable *z*

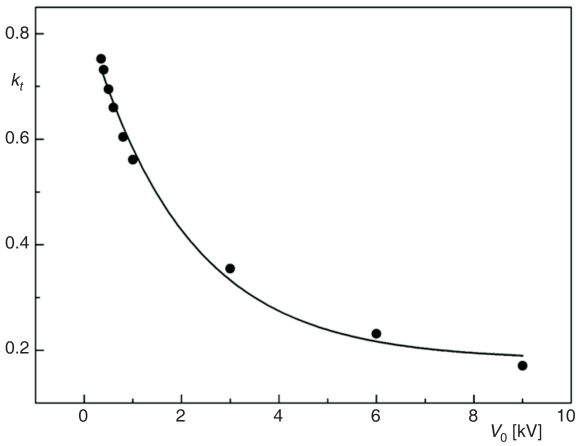

Figure 6. Dependency of the transmission coefficient k_t on potential V_0

CONCLUSIONS

We have studied the spatial rainbows patterns occurring in the transmission of a parallel proton beam of initial kinetic energy of 10 keV through an electrostatic octopole lens. The analysis was performed for biasing potentials of $V_0 = 0.35$ kV and 9.0 kV, at which the formation of the first and the second rainbow line is completed in both, the entrance and exit plain of the lens. The first RL represents a cusped square while the second is a complex one possessing 12 cusps. The focused protons of the beam are confined within the first RL which determines the shape of the beam core. The second RL defines the outer shape of the beam, consisting mostly of defocused protons. Since the proton yield abruptly changes across the RL in the exit plain, we conclude that the rainbow effect possesses typical catastrophic characteristics and can be described by the catastrophe theory.

Applying the catastrophe theory for the electrode biasing potential of $V_0 = 0.35$ kV, parameters $a(z)$ and $b(z)$ of the octopole generating function at different distances in the drift space, were determined. These parameters define the optical properties of the electrostatic octopole, because they are related to the path deviations of the third- and fifth-order in proton transmission through the lens. The dependence of the mapping parameters, *a* and *b*, on the variable *z*, can be excellently fitted with the exponential functions $a(z) = a_1 - a_2 \exp(-z/a_z)$ and $b(z) = b_1 - b_2 \exp(-z/b_z)$, where $a_1 = 0.26$ cm^{-1}, $a_2 = 0.54$ cm^{-1}, and $a_z = 29.10$ cm, and

$b_1 = 0.09$ cm^{-2}, $b_2 = 0.25$ cm^{-2}, and $b_z = 37.18$ cm. Analysis also showed that the dependency of the transmission coefficient k_t on the potential V_0 can be fitted by the exponential function $k_t(V_0) = k_1 + k_2 \exp(-V_0/k_{V_0})$, with $k_1 = 0.18$, $k_2 = 0.65$, and $k_{V_0} = 2$ kV. For $V_0 = 0.35$ kV the value of k_t is 0.75 while for $V_0 = 9$ kV k_t falls to 0.17 *i*. *e*. 4.5 times less protons are transmitted for $V_0 = 9$ kV compared to $V_0 = 0.35$ kV.

ACKNOWLEDGMENT

We acknowledge the support to this work provided by the Ministry of Education, Science and Technological Development of the Republic of Serbia through the project Physics and Chemistry with Ion Beams, No. III 45006.

AUTHORS' CONTRIBUTIONS

The idea for this research was initiated by S. M. Petrović. Computations were carried out by I. N. Telečki, and S. Grujović Zdolšek. The manuscript was written by I. N. Telečki.

REFERENCES

[1] Friedman, M. H., *et al*., Fundamentals of Ion Motion in Electric Radiofrequency Multipole Fields, *Phys. E: Sci. Instrum., 15* (1982), Jan., pp. 53 -61
[2] Gerlich, D., (editors, Cheuk-Yiu, Ng. and Baer. M)., State-Selected and State-to-State Ion-Molecule Reaction Dynamics. Part 1, Experiment, *Advances in Chemical Physics, 82* (1992), Jan., pp. 1-176
[3] Dawson, P. H., Quadrupole Mass Spectrometry and its Applications, Amsterdam: Elsevier, 1976, p. 372
[4] Rose, H., Geometrical Charged-Particle Optics, Springer-Verlag, Berlin Heidelberg, 2013, p. 518
[5] Yavor, S. Ya., *et al*., Correction of Geometrical Aberrations in Electron-Optical System by Octoupoles, *Nucl. Instrum. Meth., 99* (1972), Aug., pp. 103-108
[6] Joachim, Z., Maximilian, H., Aberration Correction in a Low Voltage SEM by a Multipole Corrector, *Nucl. Instrum.Meth. A, 363* (1995), 1-2, pp. 316-325
[7] Rose, H., Historical Aspects of Aberration Correction, *Journal of Electron Microscopy, 58* (2009), 3, pp. 77-85
[8] Telečki, I., *et al*., Spatial Rainbows and Catastrophes in Transmission of Protons through Electrostatic Hexapole Lens, *Nucl Technol Radiat, 33* (2018), 3, pp. 231-238
[9] Press, W. H., *et al*., Numerical Recipes in FORTRAN, Cambridge University Press, Cambridge, UK, 1993, p. 973
[10] Nešković, N., *et al*., A Square Electro static Rainbow Lens: Catastrophic Ion Beam Focusing, *Nucl. Instru. Meth. A, 635* (2011), 1, pp. 1-7
[11] Telečki, I., *et al*., Focusing Properties of a Square Electrostatic Rainbow Lens, *Nucl. Instr. Meth. A, 694* (2012), Dec., pp. 224-233
[12] Nešković, N., *et al.*, Rainbow Lenses, *Advances in Imaging and Electron Physics, 182* (2014), Apr., pp. 123-186
[13] Telečki, I., *et al*., Focusing Properties of a Square Electrostatic Rainbow Lens Doublet, *Nucl Technol Radiat, 30* (2015), 4, pp. 239-248
[14] Berry, M. V., Stable and Unstable Airy-Related Caustics and Beams, *J. Opt., 19* (2017), 5, pp. 1-7
[15] Poston, T., Stewart, I., Catastrophe Theory and its Applications, London: Pitman, 1978, p. 420
[16] Nye, J. F., Natural Focusing and Fine Structure of Light, IOP Publishing Ltd, 1999, p. 318
[17] Gilmore, R., Catastrophe Theory for Scientists and Engineers, John Wiley & Sons, New York, 1981, p. 666
[18] Erni, R., Aberration-Corrected Imaging in Transmission Electron Microscopy, Imperial College Press, 2010, p. 348

Received on September 10, 2018
Accepted on October 3, 2018

Игор Н. ТЕЛЕЧКИ, Сања М. ГРУЈОВИЋ ЗДОЛШЕК, Срђан М. ПЕТРОВИЋ

ПРОСТОРНЕ ДУГЕ И КАТАСТРОФЕ У ТРАНСМИСИЈИ ПРОТОНА КРОЗ ЕЛЕКТРОСТАТИЧКО ОКТОПОЛНО СОЧИВО

У овом раду посматрана је трансмисија почетног паралелног протонског снопа кинетичке енергије 10 keV кроз електростатичко октополно сочиво. Површинске дуге и одговарајуће расподеле протона рачунате су користећи апроксимативан модел потенцијала бесконачног октопола. Позитивни потенцијал на електродама сочива био је постављен на 0.35 kV и 9 kV. Показано је да се применом теорије катастрофе може одредити генерисана функција која пресликавањем позиције протона са улазне равни на позиције у трансверзалим равнима ван сочива даје индентичне линије дуге у обе равни са линијама дуге нумерички израчунате у случају кад је потенцијал на електродама био 0.35 kV.

Кључне речи: октопол, јонска оптика, теорија катастрофе, линија дуге, аберација